Transmembrane Protein 108 Inhibits the Proliferation and Myelination of Oligodendrocyte Lineage Cells in the Corpus Callosum

Yongqiang Wu
Nanchang University
Yanzi Zhong
Nanchang University
Xufeng Liao
Nanchang University
Xiangguang Miao
Nanchang University
Jianbo Yu
Nanchang University
Xinsheng Lai
Nanchang University
Yu Zhang
Nanchang University
Chaolin Ma
Nanchang University
Shunqi Wang (wsqi@ncu.edu.cn)
Nanchang University https://orcid.org/0000-0002-4918-6550

Research Article

Keywords: Tmem108, Oligodendrocyte, Myelination, Corpus callosum, Bipolar disorder

Posted Date: October 1st, 2021

DOI: https://doi.org/10.21203/rs.3.rs-942005/v1

Version of Record: A version of this preprint was published at Molecular Brain on April 11th, 2022. See the published version at https://doi.org/10.1186/s13041-022-00918-7.

Abstract

Background: Abnormal white matter is a common neurobiological change in bipolar disorder, and dysregulation of myelination in oligodendrocytes is the cause. Transmembrane protein 108 (*Tmem108*), as a susceptible gene of bipolar disorder, is expressed higher in oligodendrocyte lineage cells than any other lineage cells in the central nervous system. Moreover, *Tmem108* mutant mice exhibit mania-like behaviors, belonging to one of the signs of bipolar disorder. However, it is unknown whether *Tmem108* regulates myelination of the oligodendrocytes.

Results: *Tmem108* expression in the corpus callosum decreased with the development, and hypermyelination of the corpus callosum was found in *Tmem108* mutant mice, accompanying high expression of myelin basic protein. Strikingly, both oligodendrocyte progenitor cell proliferation and oligodendrocyte myelination were enhanced in the mutant mice. Furthermore, the mutant mice exhibited mania-like behavior after acute restraint stress and were susceptible to drug-induced epilepsy.

Conclusions: *Tmem108* inhibited oligodendrocyte progenitor cell proliferation and mitigated oligodendrocyte maturation in the corpus callosum, which may also provide a new role of *Tmem108* involving bipolar disorder pathogenesis.

Introduction

Bipolar disorder (BD) is a severe mental disease characterized by manic states being usually interspersed with periods of depression [1], affecting 1%-1.5% of the population [1, 2]. Aberrant white matter microstructure is proposed as a mechanism underlying BD, including the dimension of irritability and widespread increases in radial diffusivity [3–5]. Abnormal white matter connectivity may be associated with BD pathophysiology [4, 6], and elevated rates of white matter hyperintensities are widely observed in BD [3–5].

The CC is the brain's major white matter fiber tract [6, 7], containing most axonal transmissions between the two cerebral hemispheres. The CC develops the last brain structure to complete myelination, which is also a period accompanying the peak onset of BD [8]. Anatomical abnormalities in the CC have been reported in magnetic resonance imaging studies in BD patients, possibly because of altered myelination leading to impaired interhemispheric communication [9]. Changes in area and thickness in the corpus callosum (CC) have been reported in BD, and neuropathological data and imaging suggest possible abnormalities in myelination and glial function [2, 8]. Given the strong genetic underpinnings of both BD and white matter microstructure, such whiter matter aberrations may be a disease marker and an endophenotype of BD [3, 10].

Several genome-wide association studies (GWAS) suggest that *Tmem108* is a susceptible gene of BD[11–13], and the relevant single nucleotide polymorphism (SNP) site is not in the coding region of *Tmem108*, which is speculated that the SNP may affect its expression[13, 14]. Strikingly, the recent GWAS screened BD risk loci in the Han Chinese population, covering 1822 BD patients and 4650 control

individuals, and the data was replicated analysis. After finally multiple analyses between Han Chinese and European populations, a new SNP (rs9863544) in BD patients were found, locating in the upstream regulatory region of the *Tmem108* gene [13]. *Tmem108* expression change may be one of the onset reasons for BD.

Our previous research found that adult neurogenesis is impaired in *Tmem108* mutant mice, and manic behavior is found in the mutant mice [15], indicating that *Tmem108* also is related to BD. Furthermore, RNA sequencing showed that *Tmem108* expression is much higher in newly formed OLs than in other cells in the central nervous system (CNS) [16]. Therefore, these studies indicate that *Tmem108* may play an essential role in OLs development and myelination.

In this study, *Tmem108* expression in the corpus callosum (CC) was higher in young mice than in adult mice and colocalized with OLs in young mice CC, implying promising function in myelination with the development. Intriguingly, myelin basic protein (MBP) was highly expressed in *Tmem108* mutant mice in immunohistochemistry (IHC) staining, and western blots (WB) assay and electron microscopes revealed hypermyelination in the CC of the mutant mice, especially early-onset myelination in small axons. Consistently, the cytological experiment showed that *Tmem108* inhibited OL progenitor cell (OPC) proliferation and mitigated the maturation of CC OLs by preventing the myelination of small-diameter axons. One of the possible mechanisms might be the Wnt signaling pathway, partially similar to the regulation in adult neurogenesis [15]. Moreover, *Tmem108* mutant mice exhibited manic behavior after acute restraint stress and were susceptible to drug-induced epilepsy. This study disclosed the function of *Tmem108* in CC, which may also provide a new role of *Tmem108* involving BD pathogenesis via regulating the myelination.

Materials And Methods

Animals

Tmem108 mutant (*Tmem108-LacZ*; MMRRC: 032633-UCD) mice were described previously [15, 17, 18]. In brief, the first coding exon of *Tmem108* was replaced with the β-galactosidase/neomycin cassette. *Tmem108* mutant mice in the paper were *Tmem108-LacZ* homozygous (*Tmem108* -/-). Mice were feed in a room 12-h light/dark cycle, at 22–25℃, with ad libitum access to rodent chow diet and clean water. The experimental protocols were performed according to the "guidelines for the care and use of experimental animals" issued by Nanchang University for research about vertebrate animals. For *in vivo* experiment, surgery was performed with sodium pentobarbital anesthesia (50 mg/kg, intraperitoneal injection), and efforts were executed to minimize suffering and reduce the animal number. After the terminal experiments, mice were euthanized by carbon dioxide inhalation.

Reagents

X-gal (5-Bromo-4-chloro-3-indolyl-β-D-galactopyranoside) was purchased from Sigma-Aldrich (B4252, 30 mg/ml for staining); Pilocarpine hydrochloride and scopolamine methyl-bromide were also purchased from Sigma-Aldrich; Other chemicals were purchased from Sangon Biotech (BBI Life Sciences CO. China).

Antibodies information as follows: Rabbit anti-β-Actin antibody (Santa Cruz Biotechnology, sc-1616-R; 1:2000 for blotting); Rat anti-MBP antibody (Millipore, MAB386; 1:2000 for blotting; 1:1000 for staining); Rabbit anti-TMEM108 antibody (1:1000 for blotting) was kindly presented by Dr. J. Liu [19]; Goat anti-rabbit IgG poly-HRP secondary antibody (32260) and Goat anti-rat IgG poly-HRP secondary antibody (31471) were purchased from Thermo Fisher Scientific (1:2000 for blotting); Mouse anti-Ki67 (BD Biosciences, 550609; 1:1000 for staining); Rabbit anti-Olig2 antibody (Millipore, AB9610, 1:1000 for staining); Mouse anti-APC antibody (CC1, Millipore Sigma, MABC200, 1:800 for staining) (Tracy J Yuen 2014 Cell); Alexa Fluor 488 goat anti-rabbit lgG (Thermo Fisher Scientific, A32731; 1:1000 for staining), Alexa Fluor 568 goat anti-mouse lgG (Thermo Fisher Scientific, A-11031; 1:1000 for staining).

Behavioral analysis

For the forced swimming test (FST), mice were forced to swim in a two-liter beaker filled with about fifteen-centimeter-height water for 6 min. A camera monitored mice movements with tracking software (Video freeze version 2.5.5.0, Med Associate Inc.). The immobility in the last four min was obtained for statistical analysis.

The pilocarpine model was conducted according to the previous study [20, 21]. In order to minimize the peripheral side effects, mice were injected with scopolamine methyl-bromide (2 mg/kg mice weight, intraperitoneal injection) 30 min before pilocarpine hydrochloride (dissolved in 0.9% saline, 200 mg/kg mice weight, intraperitoneal injection) treatment. Then, mice were injected with pilocarpine (100 mg/kg mice weight) every 30 min. Behavioral seizure score was according to the criteria by Racine [20]: stage 0, no seizure; stage 1, head nodding; stage 2, sporadic full-body shaking and spasms; stage 3, chronic full-body spasms; stage 4, jumping, shrieking, and falling over; stage 5, violent convulsions, falling over and dying.

Western blots (WB)

WB was conducted as our previous research, and whiter matter (CC and medulla) and gray matter (top layers of cortex) separation were according to the previous study [22]. We homogenized the tissues in lysis buffer (0.1% SDS, 0.5% sodium deoxycholate, 1% NP-40, 1 mM EDTA, 1 mM PMSF, 1 mg/ml aprotinin, leupeptin, and pepstatin A protease inhibitors, in 1×DPBS). The protein was separated by SDS-PAGE and then transferred to a nitrocellulose membrane. After being blocked, the membrane was incubated with primary antibody and HRP-coupled secondary antibody in turn. In the last, the immunoreacted bands were captured by an enhanced chemiluminescence system (Bio RAD), and the band intensities were performed with ImageJ software.

Immunohistochemistry (IHC) staining

The mice brain's coronal sections (30 μm) were prepared by microtome (Leica CM1950) for IHC. After incubated in a citrate buffer for antigen repair, sections were permeabilized with a 20% tween for 20 min. Next, the sections were blocked for 1 h at room temperature and then incubated with primary antibody at 4°C overnight. Afterward, sections were exposed to the secondary antibody for 2 h in the dark at room temperature. Finally, the sections were transferred to the slides and mounted with coverslips. The images were captured with an inverted fluorescence microscope (Olympus FSX100). DAPI was used to identify the cellular nuclei.

Quantitative real-time PCR (qPCR)

Total RNA was isolated from mice brains according to the manufacturer's instructions of TRIzol Reagent (Invitrogen), and complementary DNA (cDNA) was synthesized following the manufacturer's protocol of High-Capacity cDNA Reverse Transcription Kit (Thermo Fisher Scientific, 4368814). The qPCR primer sets as below: *Tmem108* (5'-CCTGAGCTACTGGAACAATGCC-3' and 5'-CAGTGTCTCGATAGTCGCCAT TG-3'), and *Gapdh* (5'-CATCACTGCCACCCAGAAGACTG-3' and 5'-ATGCCAGTGAGCTTCCCGTTCAG-3'). qPCR was carried out by the StepOnePlus Real-Time PCR system (Applied Biosystems) using the mix. qPCR was performed as described previously [23]. Expression levels of mRNA were normalized to the reference gene Gapdh using a ΔCT method.

X-gal staining

X-gal is an inert chromogenic substrate for β-gal, and β-gal hydrolyzes X-gal into colorless galactose and 4-chloro-3-brom-indigo, forming an intense blue precipitate. X-gal staining was carried out as our previous study [15, 24]. In brief, the coronal sections of *Tmem108* mutant mice were prepared by microtome (Leica CM1950) and permeabilized with a detergent solution (0.01% sodium deoxycholate, 0.02% NP-40, 2 mM MgCl2 in 0.1 M pH 7.4 phosphate buffer) at 4°C. After incubated in staining solution (5 mM potassium ferricyanide, 5 mM potassium ferrocyanide, 2 mg/ml X-gal in detergent solution) overnight at 37°C, the sections were transferred to the slides and mounted with coverslips. Finally, the images were captured with an inverted fluorescence microscope (Olympus FSX100).

Electron Microscopy

For electron microscopy, young (P14) and adult (P60) male mice were perfused through the heart with phosphate buffer (PB 0.1 M, pH 7.4) followed by 2% paraformaldehyde with 0.5% glutaraldehyde in PB. After carefully dissecting the brain, the CC was immediately put into 2.5% glutaraldehyde incubating overnight at 4°C and rinsed in PB 5 min triple times. Then at room temperature, the CC was postfixed in1% osmium tetroxide for 1 h, dehydrated through 30% and 50% ethanol 15 min in turn, and immersed in 70% uranyl acetate saturating ethanol overnight. Afterward, the sample was dehydrated through 80% and 95% ethanol 15 min, in turn, followed by incubation of 100% ethanol 40 min twice. The dehydrated

sample was infiltrated in epoxypropane (30 min), epoxypropane:ethoxyline resin (1:1, 2 h), epoxypropane:ethoxyline resin (1:2, 1 h), and ethoxyline resin (Ephon812, 2 h) in a gelatin capsule in turn. Then, the sample was polymerized in an oven at 45°C 12 h and 65°C 48 h. Next, ultra-thin sections (70 nm) of the transversal cut CC axons were prepared on an ultramicrotome (LKB-Nova, Sweden). The sections were transferred onto 100 mesh copper grids followed rinsed with ddH_2O 15 min triple times and stained in lead citrate 15 min followed with ddH_2O 10 min triple times. Finally, the sections on the grids were examined on a transmission electron microscope (JEOL, JEM-2100, Japan). The *g*-ratio of a myelinated axon was calculated as the axonal diameter and fiber diameter ratio.

Statistical analysis

Values of all data are mean ± SEM (standard error of the mean). Statistical analysis was carried out by GraphPad Prism 6.01. The statistical significance between the mutant and control mice was calculated by two-way ANOVA (analysis of variance) and a two-tailed student t-test. The difference was defined as significant if the p-value < 0.05.

Results

High expression of Tmem108 in OLs of the young mice CC

Tmem108 expression was verified by qPCR and WB (Fig. 1). For the whole brain of wild-type mice, qPCR results showed that *Tmem108* had a high expression in the young mice (Fig. 1A), and the protein level of *Tmem108* was similar to the mRNA level (Fig. 1B). qPCR and WB were utilized to check *Tmem108* expression in different brain areas (Fig. 1C, 1D), including cerebellum (CB), thalamus (THY), hippocampus (HP), corpus callosum (CC), cerebral cortex (CT), striatum (STR), prefrontal cortex (PFC) and olfactory bulb (OB). Though CC and STR seemed to like having a low expression of *Tmem108*, the results supported *Tmem108* expression in both areas.

The highest expression cell type in the mice brain was newly forming OLs (Fig S1) [13]. CC was considered an area with high myelinated axons, and therefore, CC was recruited to explore the role of *Tmem108* in the OL. *Tmem108* expression decreased in postnatal development in qPCR assay (Fig. 1E). Meanwhile, X-gal staining confirmed that *Tmem108* expression was higher in young mice CC than in adult mice CC (Fig. 1F). Co-staining assay suggested that X-gal was remarkably co-stained with OL marker Olig2 of CC in the young mice (Fig. 1G).

Hypermyelination of the CC in Tmem108 mutant mice

Myelin sheath can be observed by transmission electron microscopy, presenting thick, dark closed curves around myelinated axons. In this research, the myelinated axons of the CC from young and adult perfused male mice were examined under an electron microscope. The myelinated axons' ultrastructure was obtained for statistics, and the percentage of the myelinated axons in the total axons was reported.

Littermate male mice were used to minimize the background effect from other genes between the mutant mice and the control mice.

Because myelination is increasing with mice's development, it was not surprising that the percentage of the myelinated axons in the adult mice was higher than in the young mice (Fig. 2B, 2F). The *g*-ratio value of a myelinated axon is defined as the ratio of the axonal diameter and myelinated fiber diameter, considered a typical myelination indicator. *g*-ratio value of CC in the young mutant mice was lower than the control mice (Fig. 2C). In line with expectation, hypermyelination of the CC in the adult mutant mice was observed (Fig. 2G), similar to the young mutant mice. Moreover, the mean g-ratio values of the CC axons with different diameters in the mice were counted and statistically analyzed (Fig. 2D, 2H). Notably, thin fibers in the myelinated axons of adult mice CC processed a small value of *g*-ratio (Fig. 2H).

Tmem108 mitigates the maturation of CC OLs by restricting the myelination of small-diameter axons

Enhancement of OL maturation in the mutant mice was also demonstrated by electron microscopy. In the adult mice, myelin sheath was not different between the mutant and the control mice (Fig. 2E, 2K), though their *g*-ratio was distinct (Fig. 2G). The percentage of diverse diameter fibers in total myelinated axons was investigated (Fig. 2I). Strikingly, nearly half myelinated axons in the mutant mice were thin fibers, with the axon diameter no more than 600 nm (Fig. 2I), and the diameter of myelinated OLs in the mutant mice was smaller than that in the control mice (Fig. 2K).

High expression of MBP in Tmem108 mutant mice

Whole-brain MBP level in postnatal mice was quantified by WB (Fig. 3A), and MBP expression was higher in *Tmem108* mutant mice than in the control mice after postnatal. According to the previous study [22], gray matter and white matter were separated, and the latter was considered brain areas with plenty of myelinated axons. WB indicated that gray matter in the mutant mice brain had more MBP protein than in the control brain (Fig. 3B). Consistent with anticipation, MBP in CC of the mutant mice brain was higher than the control mice brain (Fig. 3C). Relative mRNA levels of *Mbp* also were examined in the postnatal mice brain (Fig S2), in gray matter and whiter matter of adult mice (Fig S2B), and CC of adult mice (Fig S2C). *Mbp* mRNA level seemed consistent with MBP protein level in the mutant mice.

Although *Tmem108* mutant did not alter the CC area (Fig. 3D, 3E), cerebral cortex structure, and the hippocampus construction (Fig S3), MBP fluorescence intensity of the brain CC in *Tmem108* mutant mice elevated (Fig. 3D, 3F).

The proliferation of OL increased in the CC of the young mutant mice

Myelination begins relatively late in the development of mice until after birth, and myelin sheaths are first seen at P11. Increased myelination occurs during neonatal development of the mice [25]. We speculated that young mice before P11 might have a high proliferation of OPCs or newly forming OLs. Therefore, the CC of young mice at P7 was co-stained in Ki67 with Olig2 (Fig. 4A). Olig2 positive cell density increased in the mutant mice (Fig. 4B), resulting from the high proliferation of the OPCs or newly forming OLs in the

mutant mice, representing by Ki67 and Olig2 double-positive cell density in the mice (Fig. 4C). It indicated that *Tmem108* inhibited OPC and newly forming OLs proliferation.

The maturation of CC OLs in Tmem108 mutant mice was enhanced

To investigate the OLs maturation in the *Tmem108* mutant mice, we utilized CC1 staining to evaluate the maturation of CC OLs in adult mice (Fig. 5A). Intriguingly, although OL density did not change in adult mice (Fig. 5B), maturation of OLs representing by Olig2 and CC1 double-positive cells increased in the mutant mice (Fig. 5C), implying that *Tmem108* mitigated the maturation of CC OLs.

Mania-like behavior and easily induced epilepsy in Tmem108 mutant mice

Tmem108 mutant mice display anti-depression behavior (mania-like) behavior in the previous study [15]. In this study, 24-h restraint stress worsened the mania behavior in FST (Fig. 6B). Over half of *Tmem108* mutant mice exhibited severe mania-like behavior during the restraint stress and died of physical exertion (Fig. 6C). Furthermore, after the restraint stress, the remaining mutant mice struggled desperately without rest in FST (Fig. 6B), indicating severe mania-like behavior in the mutant mice. Meanwhile, the control mice could be separated into the mania-like group, depressive group, and resistant group (Fig. 6B).

Due to the similarities and the behavioral manifestation between pathophysiological mechanisms and the chronic seizures for their spontaneous and recurrent characteristics, the pilocarpine injection model is considered a classic experimental protocol to mimick human temporal lobe epilepsy [26]. The pilocarpine model was utilized to evaluate the potential epilepsy of the mutant mice. In order to avoid the peripheral side effects, scopolamine block was injected before the pilocarpine treatment (Fig. 6D). The mice were observed continuously for behavioral seizures after each pilocarpine injection. *Tmem108* mutant mice quickly reached seizure stage 5 compared with the control mice (Fig. 6E,6F), indicating *Tmem108* involved the occurrence of induced epilepsy.

Discussion

Abnormal myelin development and the mental diseases

Although SCZ and BD account for 2% – 4% of the world population, the pathogenesis and treatment of SCZ and BD are unclear and unsatisfied [27, 28]. Strikingly, imaging and autopsy studies not only show that abnormal white matter is a common neurobiological change in BD and SCZ patients[4] but also reveal that SCZ patients are accompanying with dysregulation of oligodendrocyte (OL) related processes, such as myelination developmental disorder, abnormal expression of myelination gene and number changes of OLs[29, 30]. However, the molecular between abnormal myelination and the two mental diseases is unclear.

The myelin sheath is composed of bilayer lipids as the frame, with proteins embedded as one of the plasma membranes. Most of the proteins in the myelin sheath are transmembrane proteins, such as MBP and proteolipid protein. In these proteins, MBP accounts for 30% of the total myelin protein in the CNS

and is critical for myelination [31, 32]. MBP expression was enhanced in *Tmem108* mutant mice via WB and IHC staining, and the mutant mice also exhibited hypermyelination by electron microscopy.

The myelin sheath in mature OL acts as an external insulator for current conduction, facilitating rapid saltatory impulse conduction with reduced axonal diameters. Moreover, myelin also provides essential nutritional support for myelinated neurons. Myelinated fibers are widely distributed in the brain, and myelin sheath is essential for maintaining neural circuits. Accordingly, hypomyelination or hypermyelination of OL deriving from abnormal myelination may be one of the bases of cognitive impairment in SCZ and BD, also relating to poor prognosis [29, 33].

Potential multiple functions of Tmem108 in the CNS

Tmem108, also known as Retrolinkin [19, 34, 35], is located on human chromosome 3q21. GWAS found that TMEM108 is not only related to substance addiction [36], smoking withdrawal [37], and alcohol addiction [38–41], but also is a susceptibility gene of SCZ [11, 12, 14] and BD [11–13].

O'Donovan *et al.* found that the SNP (rs7624858) mutation in the intron of *Tmem108* is related to SCZ [14] and speculated that the site caused *Tmem108* to become a susceptibility gene of SCZ by affecting gene expression. Jiao *et al.* disclosed that *Tmem108* mutant mice are impaired in spatial memory, and fear startles contextual memory and is more sensitive in PPI performance [17], a classic and plausible psychophysiological measurement of sensorimotor gating for SCZ in rodents and humans [42, 43].

The nature of the severe mental illness has been debated for more than one century. According to the prevailing manuals, International Classification of Diseases, BD, and schizophrenia reveal striking similarities, and the difference is that sensory gating and cognitive impairments are less pronounced in BD patients [44]. BD and schizophrenia consistently ranked among the leading causes of disability worldwide [45, 46], with similarities across multiple levels, such as overlapping brain structural [47, 48] and shared genetic risk factors [49–52]. BD and schizophrenia are severe psychiatric disorders with high heritability, but to date, unknown etiology, sharing genetic risk factors, and a possible illness mechanism is abnormal myelination [10, 53, 54].

Although *Tmem108* mutant impairs adult neurogenesis of the mice, it does not induce depression-like behavior but stirs manic-like behavior, suggesting *Tmem108* is higher correlating with BD than depression [15]. Strikingly, one recent GWAS screened BD risk loci in the Han Chinese population, covering 1822 BD patients and 4650 control individuals, and the data was replicated analysis. After finally multiple analyses between Han Chinese and European populations, a new SNP (rs9863544) in BD patients were found, locating in the upstream regulatory region of the *Tmem108* gene [13]. *Tmem108* expression change may be one of the onset reasons of the related psychiatry diseases.

Researchers have debated whether severe, chronic irritability without episodic mania constitutes a developmental phenotype of BD [5]. Neurobiological models of BD emphasize white matter aberrant

development, and white matter microstructure is often described as fractional anisotropy, which is positively associated with the smaller axon diameter and increased axon packing density [5].

The potential molecular mechanism of Tmem108 regulating myelination

In 2014, Zhang Y *et al.* purified eight representative cell populations in the CNS and generated the RNA transcriptome database for the different types of cells [16]. Intriguingly, *Tmem108* is expressed in the neurons as in previous research and has a higher expression in the OL lineage cells than in the neurons, significantly much higher in newly formed OL than in any other cells (Fig. S1). *Tmem108* mutant mice had manic-like behavior and were more active than the control group in forced swimming and tail suspension experiments [15]. Moreover, 24-hour restraint exacerbated the manic-like behavior of the mutant mice, and the mutant mice were easily induced epilepsy by pilocarpine, which may be partially related to the abnormal myelination.

Although *Tmem108* expression was low in the CC of the mice without detectable by X-gal staining, its expression was high in young wild-type mice and could be colocalized with Olig2 positive cells by utilizing the gene reporter mice. To explore how *Tmem108* inhibited proliferation and myelination of OL cells, gene expression with myelination regulation [55] was detected by qPCR. Intriguingly, Tcf4 was also expressed highly besides myelin regulatory factor (Myrf) in all three brain areas of *Tmem108* mutant mice (Fig S4). In previous research, *Tmem108* was reported to involve adult neurogenesis by the Wnt signaling pathway. In CC, most genes with significantly altering expression were downstream of the Wnt signaling pathway, such as Id2, Id4, Tcf4, and Tcf7l2.

Wnt signaling plays a complicated role in the OL myelination, depending on the final effector in the signaling pathway. Canonical Wnt/β-catenin signaling pathway strongly inhibits differentiation [56–58]. Under Wnt3a treatment, differentiation of OPC is strongly delayed or blocked [58], recruiting Tcf4/Tcf7l2 to β-catenin target genes to promote proliferation [57, 59]. ID2 and ID4 are regarded as the potential targets of Wnt/β-catenin/Tcf4 signals in OL development.

Not surprisingly, β-catenin decrease leads to enhancing the premyelinating OL. However, OL differentiation is not enhanced but reduced in Tcf7l2 knockout mice [56, 59], and differentiation is delayed in β-catenin inactivated mice [60], indicating the complexity of β-catenin /Tcf7l2. The potential mechanism is Tcf7l2 interacting with HDAC1 (Histone deacetylases 1) and HDAC2, which repress the expression of differentiation inhibitors [56]. Thereby, Tcf7l2 acts like a molecular switch, blocking or promoting OL differentiation by associating with the different binding partners [61]. We speculated that *Tmem108* regulated proliferation and myelination via the Wnt signaling pathway depending on different effectors, which needs further research *in vivo* and *in vitro*.

Conclusion

This study disclosed that *Tmem108* inhibited OPC proliferation and mitigated the maturation of CC OLs, which may also provide a new role of *Tmem108* as a BD risk gene via regulating myelination.

Abbreviations

ANOVA: Analysis of variance; BD: Bipolar disorder; CB: Cerebellum; CC: Corpus callosum; CNS: Central nervous system; CT: Cerebral cortex; GWAS: Genome-wide association study; FST: Forced swimming test; HP: Hippocampus; IHC: Immunohistochemistry; MBP: Myelin basic protein; OB: Olfactory bulb; OL: Oligodendrocyte; OPC: OL progenitor cell; PFC: Prefrontal cortex; PPI: Pre-pulse inhibition test; qPCR: quantitative real-time PCR; SEM: Standard error of the mean; SNP: Single nucleotide polymorphism; STR: Striatum; SCZ: Schizophrenia; *Tmem108*: Transmembrane protein 108; THY: Thalamus; WB: Western blots; X-gal: 5-Bromo-4-chloro-3-indolyl-β-D-galactopyranoside.

Declarations

Acknowledgments

We thank Dr. Baoming Li (Institute of Psychological Sciences, Hangzhou Normal University), Dr. Bingxing Pan, Dr. Erkang Fei, and Dr. Suqi Zou (Institute of Life Science, Nanchang University) for assisting in this project. Thanks to Dr. Jiajia Liu (Institute of Genetics and Developmental Biology, Chinese Academy of Sciences) for providing the TMEM108 antibody and Dr. Shiwen Luo (Medical School of Jiangxi, Nanchang University) and Dr. Huifeng Jiao (School of Basic Medical Science, Nanchang University) for suggestions *Tmem108* research.

Author Contributions

S Wang initiated and designed the study. J Yu and X Liao performed a glucose tolerance test, insulin resistance test, behavior test, and qPCR. J Yu and Y Zhong performed the metabolism test. Y Wu and D Lin assisted in the animal test. Y Zhang and D Ren cultured mice. S Zou, X Lai, E Fei, and C Ma analyzed data. H Jiao and M Yan advised on the project. S Wang wrote the manuscript with input from all coauthors. All authors have read and agreed to the published version of the manuscript.

Funding

This work was supported partly by grants from China's National Natural Science Foundation (31760276, 31960171, 31460260) and the Jiangxi Natural Science Foundation (20171BAB204019 20192ACB20022).

Availability of Data and Materials

The datasets used or analyzed in our study are available from the corresponding author on reasonable request.

Ethics Approval and Consent to Participate

All experiments involving animals were conducted according to the "guidelines for the care and use of experimental animals" issued by Nanchang University. The Committee on the Ethics of Animal

Experiments of the University of Nanchang approved the protocol.

Consent for Publication

Not applicable

Competing Interests

The authors have no conflicts of interest to declare.

References

1. Mahon, K., K.E. Burdickand P.R. Szeszko. A role for white matter abnormalities in the pathophysiology of bipolar disorder. Neurosci Biobehav Rev. 2010; 34(4):533-554.
2. Marlinge, E., F. Bellivierand J. Houenou. White matter alterations in bipolar disorder: potential for drug discovery and development. Bipolar Disord. 2014; 16(2):97-112.
3. Hu, R., C. Stavish, E. Leibenluftand J.O. Linke. White Matter Microstructure in Individuals With and At Risk for Bipolar Disorder: Evidence for an Endophenotype From a Voxel-Based Meta-analysis. Biol Psychiatry Cogn Neurosci Neuroimaging. 2020; 5(12):1104-1113.
4. Sehmbi, M., C.D. Rowley, L. Minuzzi, F. Kapczinski, J.M. Kwiecien, N.A. Bock, et al. Age-related deficits in intracortical myelination in young adults with bipolar disorder type I. J Psychiatry Neurosci. 2019; 44(2):79-88.
5. Linke, J.O., N.E. Adleman, J. Sarlls, A. Ross, S. Perlstein, H.R. Frank, et al. White Matter Microstructure in Pediatric Bipolar Disorder and Disruptive Mood Dysregulation Disorder. J Am Acad Child Adolesc Psychiatry. 2020; 59(10):1135-1145.
6. Bearden, C.E., T.G. van Erp, R.A. Dutton, C. Boyle, S. Madsen, E. Luders, et al. Mapping corpus callosum morphology in twin pairs discordant for bipolar disorder. Cereb Cortex. 2011; 21(10):2415-2424.
7. Caetano, S.C., C.M. Silveira, S. Kaur, M. Nicoletti, J.P. Hatch, P. Brambilla, et al. Abnormal corpus callosum myelination in pediatric bipolar patients. J Affect Disord. 2008; 108(3):297-301.
8. Lloyd, A.J., H.E. Ali, D. Nesbitt, P.B. Moore, A.H. Youngand I.N. Ferrier. Corpus callosum changes in euthymic bipolar affective disorder. Br J Psychiatry. 2014; 204(2):129-136.
9. Brambilla, P., M. Nicoletti, R.B. Sassi, A.G. Mallinger, E. Frank, M.S. Keshavan, et al. Corpus callosum signal intensity in patients with bipolar and unipolar disorder. J Neurol Neurosurg Psychiatry. 2004; 75(2):221-225.
10. Tkachev, D., M.L. Mimmack, M.M. Ryan, M. Wayland, T. Freeman, P.B. Jones, et al. Oligodendrocyte dysfunction in schizophrenia and bipolar disorder. The Lancet. 2003; 362(9386):798-805.
11. Gonzalez-Mantilla, A.J., A. Moreno-De-Luca, D.H. Ledbetterand C.L. Martin. A Cross-Disorder Method to Identify Novel Candidate Genes for Developmental Brain Disorders. JAMA Psychiatry. 2016; 73(3):275-283.

12. Moskvina, V., N. Craddock, P. Holmans, I. Nikolov, J.S. Pahwa, E. Green, et al. Gene-wide analyses of genome-wide association data sets: evidence for multiple common risk alleles for schizophrenia and bipolar disorder and for overlap in genetic risk. Mol Psychiatry. 2009; 14(3):252-260.
13. Li, H.J., C. Zhang, L. Hui, D.S. Zhou, Y. Li, C.Y. Zhang, et al. Novel Risk Loci Associated With Genetic Risk for Bipolar Disorder Among Han Chinese Individuals: A Genome-Wide Association Study and Meta-analysis. JAMA Psychiatry. 2021; 78(3):320-330.
14. O'Donovan, M.C., N. Craddock, N. Norton, H. Williams, T. Peirce, V. Moskvina, et al. Identification of loci associated with schizophrenia by genome-wide association and follow-up. Nat Genet. 2008; 40(9):1053-1055.
15. Yu, Z., D. Lin, Y. Zhong, B. Luo, S. Liu, E. Fei, et al. Transmembrane protein 108 involves in adult neurogenesis in the hippocampal dentate gyrus. Cell Biosci. 2019; 9:9.
16. Zhang, Y., K.N. Chen, S.A. Sloan, M.L. Bennett, A.R. Scholze, S. O'Keeffe, et al. An RNA-Sequencing Transcriptome and Splicing Database of Glia, Neurons, and Vascular Cells of the Cerebral Cortex. Journal of Neuroscience. 2014; 34(36):11929-11947.
17. Jiao, H.F., X.D. Sun, R. Bates, L. Xiong, L. Zhang, F. Liu, et al. Transmembrane protein 108 is required for glutamatergic transmission in dentate gyrus. Proc Natl Acad Sci U S A. 2017; 114(5):1177-1182.
18. Tang, T., L. Li, J. Tang, Y. Li, W.Y. Lin, F. Martin, et al. A mouse knockout library for secreted and transmembrane proteins. Nat Biotechnol. 2010; 28(7):749-755.
19. Liu, J.J., J. Ding, C. Wu, P. Bhagavatula, B. Cui, S. Chu, et al. Retrolinkin, a membrane protein, plays an important role in retrograde axonal transport. Proc Natl Acad Sci U S A. 2007; 104(7):2223-2228.
20. Sun, X.D., L. Li, F. Liu, Z.H. Huang, J.C. Bean, H.F. Jiao, et al. Lrp4 in astrocytes modulates glutamatergic transmission. Nat Neurosci. 2016; 19(8):1010-1018.
21. Tan, G.-H., Y.-Y. Liu, X.-L. Hu, D.-M. Yin, L. Meiand Z.-Q. Xiong. Neuregulin 1 represses limbic epileptogenesis through ErbB4 in parvalbumin-expressing interneurons. Nature Neuroscience. 2012; 15(2):258-266.
22. Tao, Y., P. Dai, Y. Liu, S. Marchetto, W.-C. Xiong, J.-P. Borg, et al. Erbin regulates NRG1 signaling and myelination. Proc Natl Acad Sci U S A. 2009; 106(23):9477-9482.
23. Wang, S., S. Huang, X. Zhao, Q. Zhang, M. Wu, F. Sun, et al. Enrichment of prostate cancer stem cells from primary prostate cancer cultures of biopsy samples. Int J Clin Exp Pathol. 2014; 7(1):184-193.
24. Yan, M., A. Guo, P. Chen, H. Jing, D. Ren, Y. Zhong, et al. LRP4 LDLalpha repeats of astrocyte enhance dendrite arborization of the neuron. Mol Brain. 2020; 13(1):166.
25. Khanbabaei, M., E. Hughes, J. Ellegood, L.R. Qiu, R. Yip, J. Dobry, et al. Precocious myelination in a mouse model of autism. Transl Psychiatry. 2019; 9(1):251.
26. de Oliveira, J.C., C. Medeiros Dde, E.R.G.H. de Souza, M.F. Moraesand V.R. Cota. Temporally unstructured electrical stimulation to the amygdala suppresses behavioral chronic seizures of the pilocarpine animal model. Epilepsy Behav. 2014; 36:159-164.

27. Van Rheenen, T.E., K.E. Lewandowski, I.E. Bauer, F. Kapczinski, K. Miskowiak, K.E. Burdick, et al. Current understandings of the trajectory and emerging correlates of cognitive impairment in bipolar disorder: An overview of evidence. Bipolar Disord. 2020; 22(1):13-27.
28. Fullerton, J.M.and J.I. Nurnberger. Polygenic risk scores in psychiatry: Will they be useful for clinicians? F1000Res. 2019; 8(F1000 Faculty Rev):1293.
29. Raabe, F.J., L. Slapakova, M.J. Rossner, L. Cantuti-Castelvetri, M. Simons, P.G. Falkai, et al. Oligodendrocytes as A New Therapeutic Target in Schizophrenia: From Histopathological Findings to Neuron-Oligodendrocyte Interaction. Cells. 2019; 8(12):1496.
30. Jiang, W., T.Z. Kingand J.A. Turner. Imaging Genetics Towards a Refined Diagnosis of Schizophrenia. Front Psychiatry. 2019; 10:494.
31. Voineskos, A.N., D. Felsky, N. Kovacevic, A.K. Tiwari, C. Zai, M.M. Chakravarty, et al. Oligodendrocyte genes, white matter tract integrity, and cognition in schizophrenia. Cereb Cortex. 2013; 23(9):2044-2057.
32. Boggs, J.M. Myelin basic protein: a multifunctional protein. Cell Mol Life Sci. 2006; 63(17):1945-1961.
33. Gouvea-Junqueira, D., A.C.B. Falvella, A. Antunes, G. Seabra, C. Brandao-Teles, D. Martins-de-Souza, et al. Novel Treatment Strategies Targeting Myelin and Oligodendrocyte Dysfunction in Schizophrenia. Front Psychiatry. 2020; 11:379.
34. Xu, C., X. Fu, S. Zhuand J.J. Liu. Retrolinkin recruits the WAVE1 protein complex to facilitate BDNF-induced TrkB endocytosis and dendrite outgrowth. Mol Biol Cell. 2016; 27(21):3342-3356.
35. Fu, X., Y. Yang, C. Xu, Y. Niu, T. Chen, Q. Zhou, et al. Retrolinkin cooperates with endophilin A1 to mediate BDNF-TrkB early endocytic trafficking and signaling from early endosomes. Mol Biol Cell. 2011; 22(19):3684-3698.
36. Johnson, C., T. Drgon, Q.R. Liu, P.W. Zhang, D. Walther, C.Y. Li, et al. Genome wide association for substance dependence: convergent results from epidemiologic and research volunteer samples. BMC Med Genet. 2008; 9:113.
37. Uhl, G.R., Q.-R. Liu, T. Drgon, C. Johnson, D. Walther, J.E. Rose, et al. Molecular Genetics of Successful Smoking Cessation Convergent Genome-Wide Association Study Results. Arch Gen Psychiatry. 2008; 65(6):683-693.
38. Heath, A.C., J.B. Whitfield, N.G. Martin, M.L. Pergadia, A.M. Goate, P.A. Lind, et al. A quantitative-trait genome-wide association study of alcoholism risk in the community: findings and implications. Biol Psychiatry. 2011; 70(6):513-518.
39. Zuo, L., J. Gelernter, C.K. Zhang, H. Zhao, L. Lu, H.R. Kranzler, et al. Genome-wide association study of alcohol dependence implicates KIAA0040 on chromosome 1q. Neuropsychopharmacology. 2012; 37(2):557-566.
40. Pei, Y.F., L. Zhang, T.L. Yang, Y. Han, R. Hai, S. Ran, et al. Genome-wide association study of copy number variants suggests LTBP1 and FGD4 are important for alcohol drinking. PLoS One. 2012; 7(1):e30860.

41. Agrawal, A.and L.J. Bierut. Identifying genetic variation for alcohol dependence. Alcohol Res. 2012; 34(3):274-281.
42. Hiroi, N.and A. Nishi. Dimensional Deconstruction and Reconstruction of CNV-Associated Neuropsychiatric Disorders. Handbook of Behavioral Neuroscience. 2016; 23:285-302.
43. Halberstadt, A.and M. Geyer. Hallucinogens. Encyclopedia of Behavioral Neuroscience. 2010(pages):12-20.
44. Maier, W., A. Zobeland M. Wagner. Schizophrenia and bipolar disorder: differences and overlaps. Curr Opin Psychiatry. 2006; 19(2):165-170.
45. Whiteford, H.A., L. Degenhardt, J. Rehm, A.J. Baxter, A.J. Ferrari, H.E. Erskine, et al. Global burden of disease attributable to mental and substance use disorders: findings from the Global Burden of Disease Study 2010. The Lancet. 2013; 382(9904):1575-1586.
46. Schafer, M., J.W. Kim, J. Joseph, J. Xu, S. Frangouand G.E. Doucet. Imaging Habenula Volume in Schizophrenia and Bipolar Disorder. Front Psychiatry. 2018; 9:456.
47. International Schizophrenia, C., S.M. Purcell, N.R. Wray, J.L. Stone, P.M. Visscher, M.C. O'Donovan, et al. Common polygenic variation contributes to risk of schizophrenia and bipolar disorder. Nature. 2009; 460(7256):748-752.
48. Lichtenstein, P., B.H. Yip, C. Björk, Y. Pawitan, T.D. Cannon, P.F. Sullivan, et al. Common genetic determinants of schizophrenia and bipolar disorder in Swedish families: a population-based study. Lancet. 2009; 373(9659):234-239.
49. van Erp, T.G.M., E. Walton, D.P. Hibar, L. Schmaal, W. Jiang, D.C. Glahn, et al. Cortical Brain Abnormalities in 4474 Individuals With Schizophrenia and 5098 Control Subjects via the Enhancing Neuro Imaging Genetics Through Meta Analysis (ENIGMA) Consortium. Biol Psychiatry. 2018; 84(9):644-654.
50. Hibar, D.P., L.T. Westlye, N.T. Doan, N. Jahanshad, J.W. Cheung, C.R.K. Ching, et al. Cortical abnormalities in bipolar disorder: an MRI analysis of 6503 individuals from the ENIGMA Bipolar Disorder Working Group. Mol Psychiatry. 2018; 23(4):932-942.
51. van Erp, T.G., D.P. Hibar, J.M. Rasmussen, D.C. Glahn, G.D. Pearlson, O.A. Andreassen, et al. Subcortical brain volume abnormalities in 2028 individuals with schizophrenia and 2540 healthy controls via the ENIGMA consortium. Mol Psychiatry. 2016; 21(4):547-53.
52. Hibar, D.P., L.T. Westlye, T.G. van Erp, J. Rasmussen, C.D. Leonardo, J. Faskowitz, et al. Subcortical volumetric abnormalities in bipolar disorder. Mol Psychiatry. 2016; 21(12):1710-1716.
53. Ji, E., F. Lejuste, S. Sarrazinand J. Houenou. From the microscope to the magnet: Disconnection in schizophrenia and bipolar disorder. Neurosci Biobehav Rev. 2019; 98:47-57.
54. Jorgensen, K.N., S. Nerland, L.B. Norbom, N.T. Doan, R. Nesvag, L. Morch-Johnsen, et al. Increased MRI-based cortical grey/white-matter contrast in sensory and motor regions in schizophrenia and bipolar disorder. Psychol Med. 2016; 46(9):1971-1985.
55. Santos, A.K., M.S. Vieira, R. Vasconcellos, V.A.M. Goulart, A.H. Kiharaand R.R. Resende. Decoding cell signalling and regulation of oligodendrocyte differentiation. Semin Cell Dev Biol. 2019; 95:54-73.

56. Ye, F., Y. Chen, T. Hoang, R.L. Montgomery, X.H. Zhao, H. Bu, et al. HDAC1 and HDAC2 regulate oligodendrocyte differentiation by disrupting the beta-catenin-TCF interaction. Nat Neurosci. 2009; 12(7):829-838.
57. Fancy, S.P., S.E. Baranzini, C. Zhao, D.I. Yuk, K.A. Irvine, S. Kaing, et al. Dysregulation of the Wnt pathway inhibits timely myelination and remyelination in the mammalian CNS. Genes Dev. 2009; 23(13):1571-1585.
58. Shimizu, T., T. Kagawa, T. Wada, Y. Muroyama, S. Takadaand K. Ikenaka. Wnt signaling controls the timing of oligodendrocyte development in the spinal cord. Dev Biol. 2005; 282(2):397-410.
59. Fu, H., S. Kesariand J. Cai. Tcf7l2 is tightly controlled during myelin formation. Cell Mol Neurobiol. 2012; 32(3):345-352.
60. Dai, J., K.K. Bercuryand W.B. Macklin. Interaction of mTOR and Erk1/2 signaling to regulate oligodendrocyte differentiation. Glia. 2014; 62(12):2096-2109.
61. Mitew, S., C.M. Hay, H. Peckham, J. Xiao, M. Koenningand B. Emery. Mechanisms regulating the development of oligodendrocytes and central nervous system myelin. Neuroscience. 2014; 276:29-47.

Figures

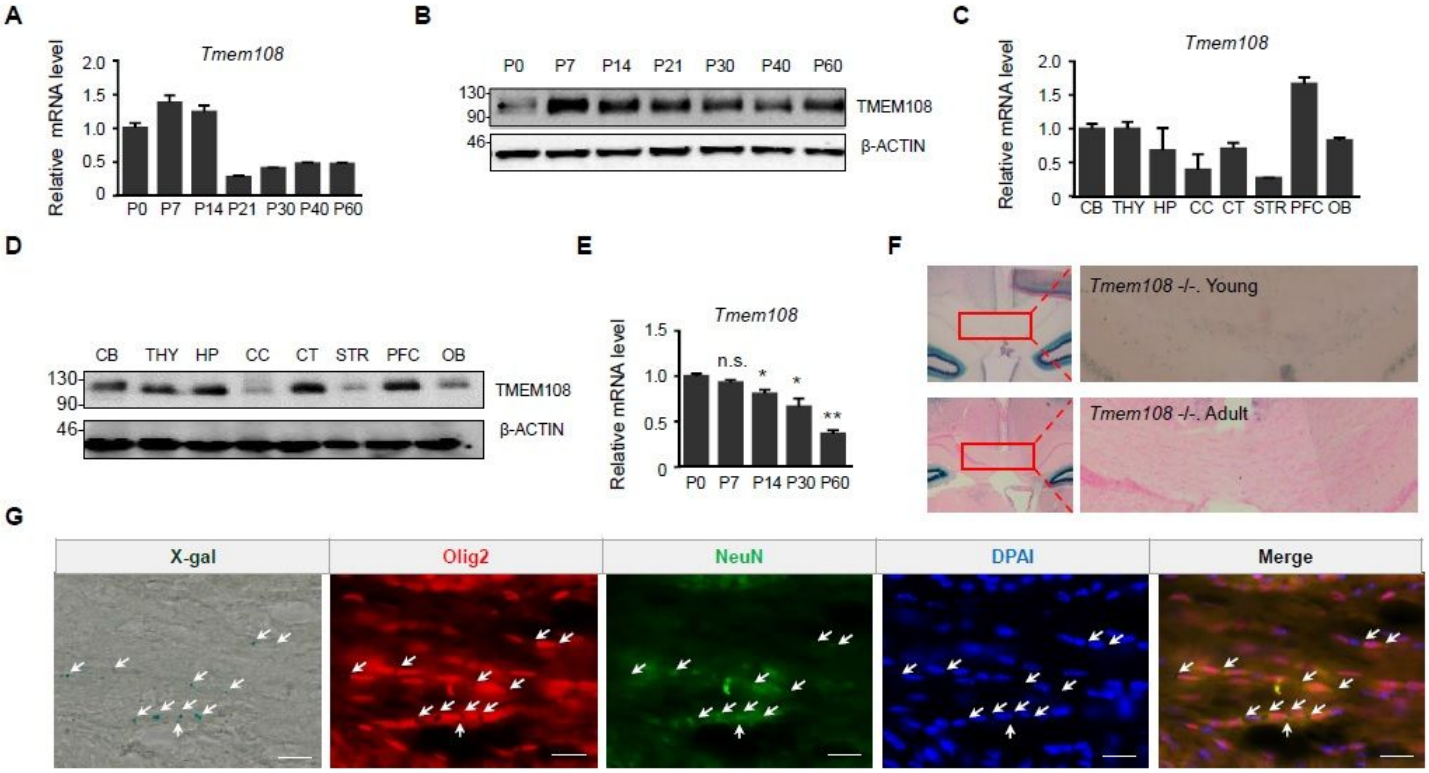

Fig 1

Figure 1

Tmem108 expression profile in several areas of the brain A. Relative expression of Tmem108 in postnatal mice brain was quantified by qPCR. Gapdh was used as an internal control (Internal control of the below is same in qPCR assay), and Tmem108 expression in P0 mice was defined as 1; Wild type male mice per group, n = 5. B. Representative image of TMEM108 level in postnatal mice brains verified by western blotting. β-ACTIN was used as an internal control (Internal control of the below is the same in western blotting). C. Tmem108 relative expression in the different areas of the adult mice brain. Tmem108 expression in CB was defined as 1; Wild type male mice, n=3; CB, cerebellum; THY, thalamus; HP, hippocampus; CC, corpus callosum; CT, cerebral cortex; STR, striatum; PFC, prefrontal cortex; OB, olfactory bulb. D. Representative image of TMEM108 level in different areas of adult mice brain verified by western blotting. E. Tmem108 relative expression of CC decreased in postnatal mice development. Tmem108 expression in P0 mice CC was defined as 1; Wild type male mice per group, n=3 (Unpaired T-test were made to compare with P0 data, n.s., not significant, * $p < 0.05$, ** $p < 0.01$). F. Tmem108 expression in young mice CC was higher than in adult mice CC by X-gal staining. Tmem108 -/- mice per group, n = 3. G. Co-staining indicated Tmem108 expression mostly colocalized with oligodendrocytes in the corpus callosum of young mice. X-gal staining represented β-gal expression downstream of the Tmem108 promoter, and the arrows showed the X-gal staining dots in Tmem108 mutant mice (P14, Tmem108 -/- mice n = 3, scale bar = 20 μm).

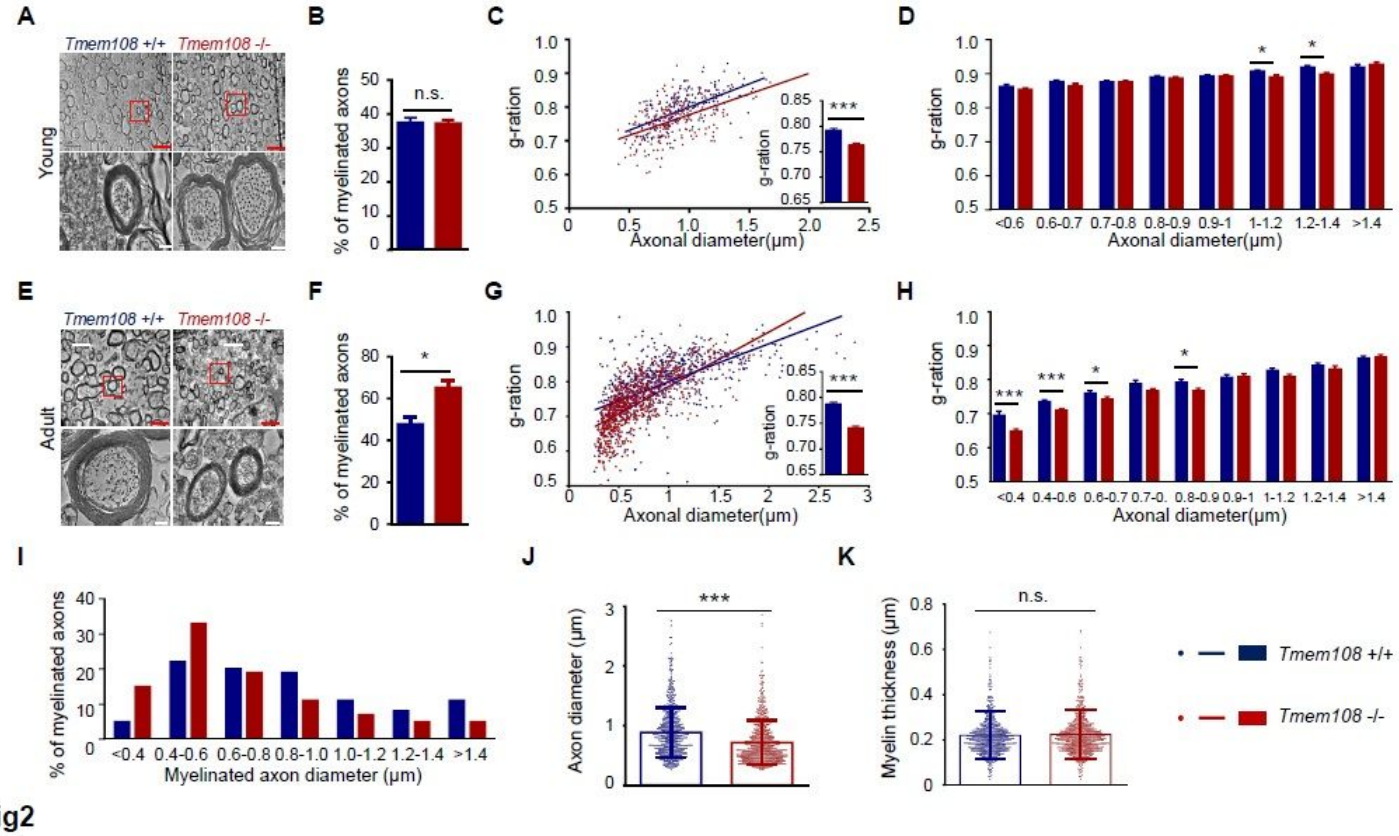

Fig2

Figure 2

Hypermyelination of the corpus callosum in Tmem108 mutant mice A. Representative electron microscopy of axons in the CC of young animals at P14. Same littermate male mice were used. B.

Percentages of CC myelinated axons were quantified in the young mice(P14). C. Scatter plot of g-ratio values and g-ratio mean in CC of the young mice(P14). D. Mean g-ratio values of CC myelinated axons with different diameters in the young mice(P14). E. Representative electron microscopy of axons in the CC of adult mice (2 M). Same littermate male mice were used. F. Percentages of CC myelinated axons were quantified in the adult mice. G. Scatter plot of g-ratio values and g-ratio mean in CC of the adult mice. H. Mean g-ratio values of CC myelinated axons with different diameters in the adult mice. (Red scale bar = 2 μm, white scale bar = 200 nm; Male mice per group n = 3, over 200 fibers per each type of animal were analyzed; Values were means ± SEM; Unpaired T-test were made between the groups; n.s., not significant, * $p < 0.05$, *** $p < 0.001$). I-K. Small-diameter CC axons in Tmem108 mutant mice were readily myelinated. I. Percentage of myelinated axons with different diameters in the total myelinated axons. J. Diameter of myelinated axons in the adult mice. K. Myelin thickness of CC axons in the adult mice (Tmem108 +/+ mice n = 3, axon fiber n = 684; Tmem108 -/- mice n =3, axon fiber n =757; Unpaired T-test were made between the groups; n.s., not significant).

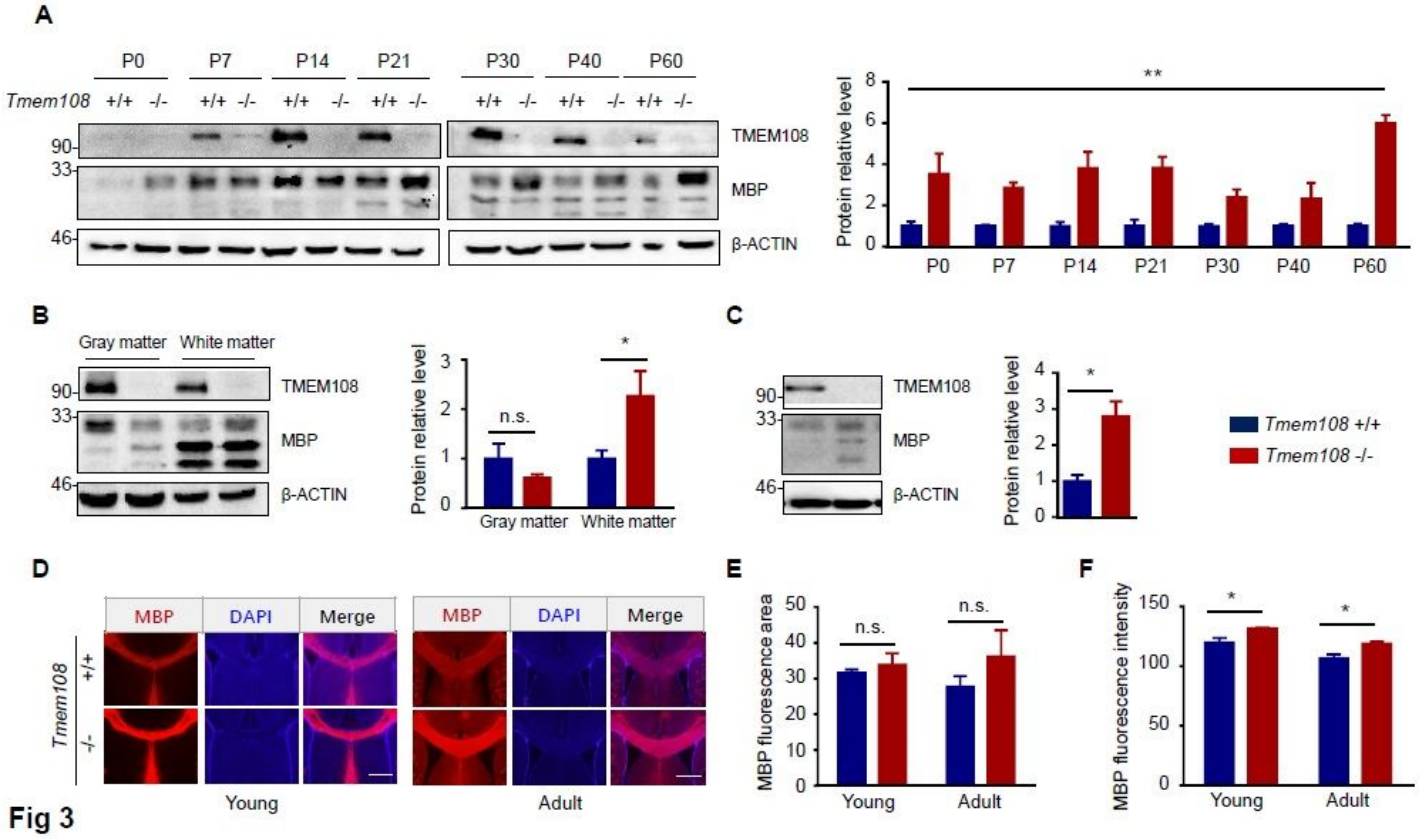

Fig 3

Figure 3

High expression of MBP in Tmem108 mutant mice A. Representative image of MBP level in postnatal mice brain by western blotting (left panel); Quantification of MBP level in the western blotting (right panel). Two-way ANOVA analysis, Tmem108 +/+ mice n = 3, Tmem108 -/- mice n = 3. B-C. Representative image of MBP level in different areas of adult mice brain by western blotting (left panel); Quantification of MBP level in the western blotting (right panel), including Gray matter, white matter (B), and CC (C) (T-test analysis, Tmem108 +/+ mice n = 5, Tmem108 -/- mice n = 5; Two-way ANOVA and unpaired T-test

analysis were used, * p < 0.05, ** p < 0.01). D-F. High MBP fluorescence intensity in the corpus callosum of Tmem108 mutant mice. D. Representative images of MBP staining in mice CC. E. MBP fluorescence area of CC in Tmem108 mutant mice (Tmem108 -/-) was not different from the control mice (Tmem108 +/+). F. MBP fluorescence intensity of CC in Tmem108 mutant mice was higher than the control mice. (Scale bar = 200 μm; Male mice per group, n = 3, unpaired T-test analysis, n.s., not significant, * p < 0.05)

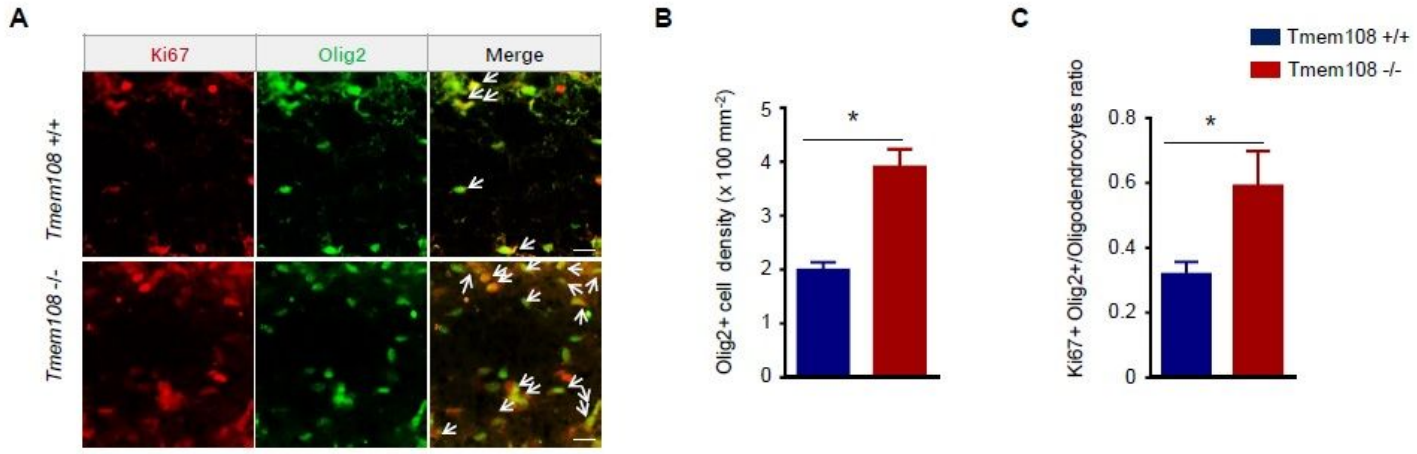

Fig 4

Figure 4

The proliferation of OL increased in the CC of the young mutant mice A. Representative images of CC in young mice at P7 co-staining Ki67 with Olig2. B. Quantified Olig2 positive cell density of CC in young mice at P7. C. Quantified double-positive (Olig2+ and Ki67+) cell density of CC in young mice at P7. (Scale bar = 20 μm; Male mice per group n = 5; Values are means ± SEM; Unpaired T-test were made between the groups; * p < 0.05)

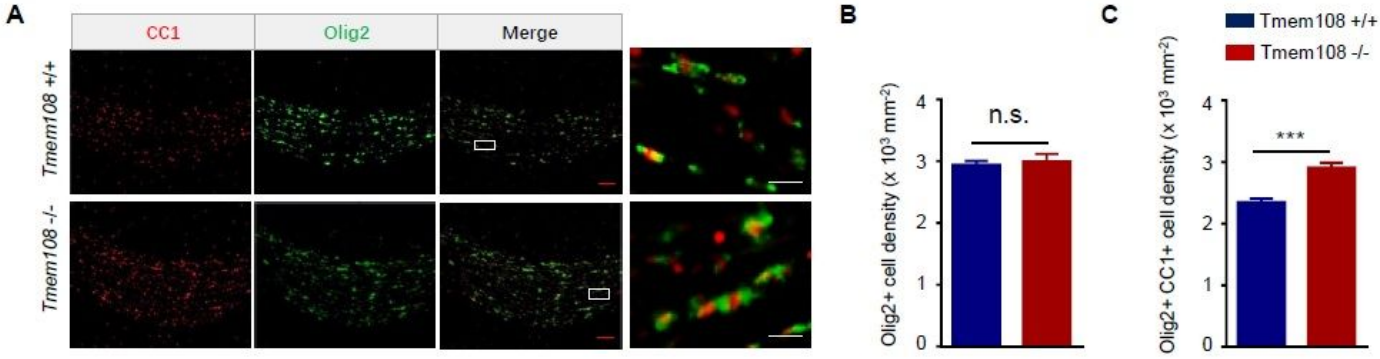

Fig 5

Figure 5

Maturation of CC oligodendrocytes in Tmem108 mutant mice increased A. Representative images of CC in the adult mice co-staining CC1 with Olig2. The dotted areas in the left panel were enlarged and shown

on the right panel. B. Quantified Olig2 positive cell density of CC in the adult mice. C. Quantified double-positive (Olig2+ and CC1+) cell density of CC in the adult mice. (Red scale bar = 50 μm, white scale bar = 10 μm; Male mice per group n = 5; Values are means ± SEM; Unpaired T-test were made between the groups; n.s., not significant, *** p < 0.001)

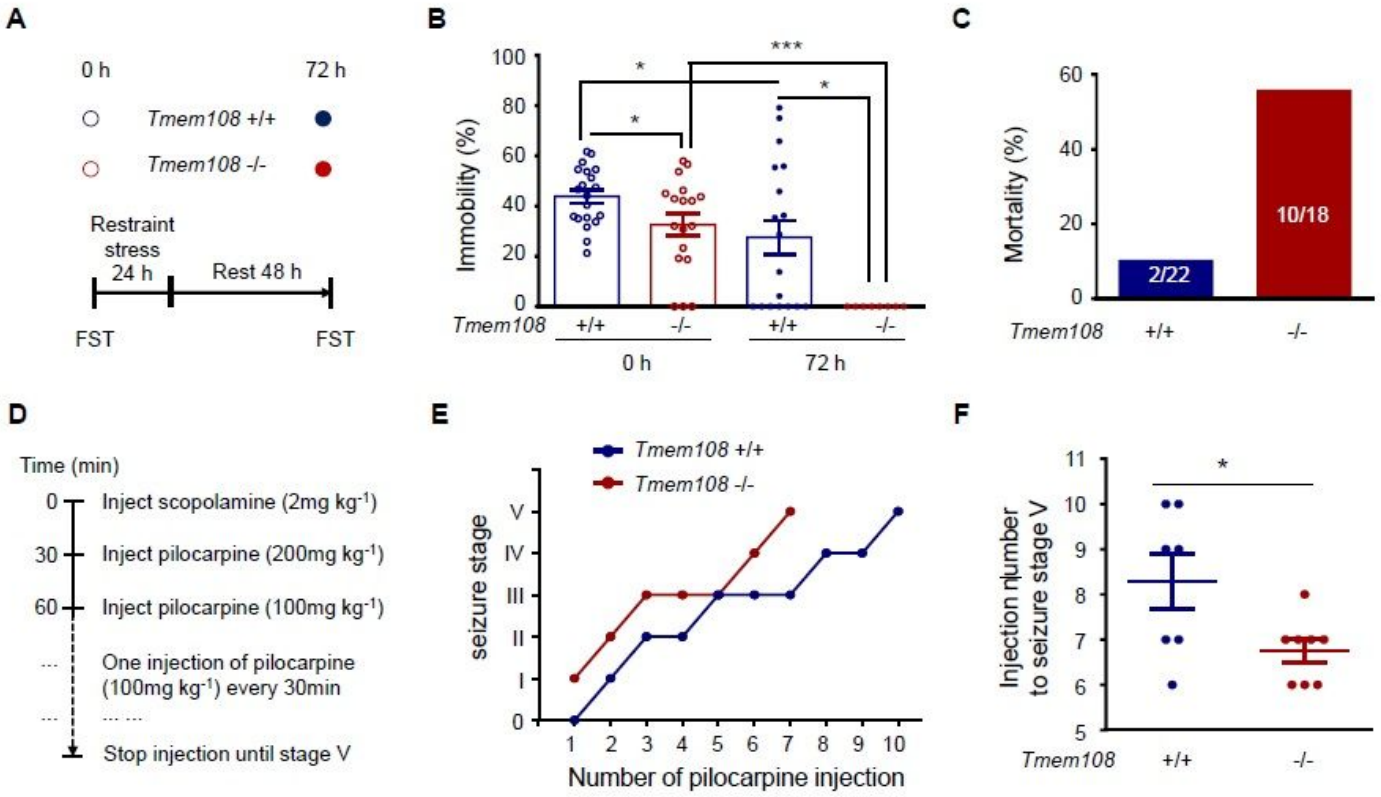

Fig 6

Figure 6

Tmem108 mutant mice exhibited mania-like behavior and were easily induced epilepsy A. Schematic of forced swimming test (FST) with restraint stress; FST were recorded before restraint stress and two-day interval after restraint stress. B. Comparing the immobility with the control mice before and after restrain stress, Tmem108 mutant (Tmem108 -/-) mice exhibited mania-like behavior in the tests (Tmem108 +/+ mice n = 22, Tmem108 -/- mice n = 18). C. Tmem108 mutant mice had serious mortality in the restraint stress. D. Schematic of seizure inducement. Scopolamine was injected 30 min before the application of pilocarpine to minimize the peripheral side effects. E. Representative time courses of seizure development by repeated pilocarpine injection. Mice of two genotypes were subjected to pilocarpine injection every 30 min and scored for the seizure stage. F. An increased number of pilocarpine injections were needed to reach stage 5 seizure for Tmem108 mutant mice (Tmem108 +/+ mice n = 7, Tmem108 -/- mice n = 8). (Unpaired T-test analysis; * p < 0.05, *** p < 0.001)

Supplementary Files

This is a list of supplementary files associated with this preprint. Click to download.

- SupplementaryFiguresandTable.pdf